An *In Situ* SEM-FIB-Based Method for Contrast Enhancement and Tomographic Reconstruction for Structural Quantification of Porous Carbon Electrodes

Santhana K. Eswara-Moorthy,[1,2,*] Prasanth Balasubramanian,[2] Willem van Mierlo,[2] Jörg Bernhard,[2] Mario Marinaro,[3] Margret Wohlfahrt-Mehrens,[3] Ludwig Jörissen,[3] and Ute Kaiser[2]

[1]*Département Science et Analyse des Matériaux (UIS), Centre de Recherche Public – Gabriel Lippmann, 41, rue du Brill, L-4422 Belvaux, Luxembourg*

[2]*Central Facility of Electron Microscopy, Group of Electron Microscopy of Material Science, Universität Ulm, 89081 Ulm, Germany*

[3]*Zentrum für Sonnenenergie- und Wasserstoff-Forschung Baden-Württemberg, 89081 Ulm, Germany*

Abstract: A new *in situ* Scanning Electron Microscope-Focused Ion Beam-based method to study porous carbon electrodes involving Pt filling of pores from gaseous precursors has been demonstrated to show drastically improved image contrast between the carbon and porous phases when compared with the Si-resin vacuum-impregnation method. Whereas, the latter method offered up to 20% contrast, the new method offers remarkably higher contrast (42%), which enabled fast semi-automated demarcation of carbon boundaries and subsequent binarization of the images with very high fidelity. Tomographic reconstruction of the porous carbon electrode was then obtained from which several morphological parameters were quantified. The porosity was found to be $72 \pm 2\%$. The axial and radial tortuosites were 1.45 ± 0.04 and 1.43 ± 0.04, respectively. Pore size, which is defined to be the distance from the medial axis of the pore to the nearest solid boundary, was quantified. Average pore size determined from the pore size distribution was 90 nm and the corresponding 1 sigma ranges from 45 to 134 nm. Surface-to-volume ratio of the carbon phase was $46.5 \, \mu m^{-1}$. The ratio of total surface area to the total volume of electrode including pores (i.e., specific surface area) was $13 \, \mu m^{-1}$.

Key words: porous carbon electrode, Pt filling, SEM-FIB, tomography, structural quantification

INTRODUCTION

Technological interest in porous carbon electrodes has recently increased for energy conversion and storage applications, such as in fuel cells and Li-air batteries (Uchida et al., 1995; Brandon & Brett, 2006; Kaiser et al., 2007; Armand & Tarascone, 2008; Lee et al., 2011). Because of their porous nature, they offer a very attractive energy-to-weight ratio. However, there are several experimental challenges that hamper technological development of these batteries and fuel cells, including the difficulty in accomplishing quantitative structural and topological characterization of the porous carbon electrode.

Structural features of the carbon electrode, such as porosity, tortuosity (ratio of the length of the pore trajectory to the distance between the ends, i.e., arc-chord ratio), and pore size distribution are crucial parameters that play a dominant role in kinetics of the electrochemical reactions (Long et al., 2004; García & Chiang, 2007). Therefore, a thorough quantitative microstructural characterization of the porous carbon electrode is indispensable for a complete understanding of the electrochemical behavior and to further develop next-generation energy technologies.

The standard approach to characterize porous samples is vacuum impregnation of the samples with an epoxy (Iwai et al., 2010). This approach works well when the electrode material under investigation is composed of chemical elements, which are significantly different than the epoxy. However, this approach does not work for carbon-based electrodes because the epoxy and the sample are chemically nearly identical and thus offer insufficient contrast to visually distinguish the impregnated epoxy from the carbon structures present in the electrode (Ender et al., 2011).

To overcome this difficulty, Ender et al. (2011) successfully used Si-based resin instead of conventional carbon-based epoxy to improve the contrast between the vacuum-impregnated material and the carbon structures alongside LiFePO$_4$ particles present in an Li-ion battery cathode. Unlike the subject of the present article, their electrodes are not exclusively porous carbon structures. Yet, it nicely illustrates that by using Si-based resin the carbon structures can be visually distinguished from other materials. They have also investigated automated quantification (Ender et al., 2012).

In this report, we show that although contrast is qualitatively better with the Si-based resin in the porous carbon, the rather weak contrast (20%) precludes accurate and robust quantification of microstructural features such as porosity, tortuosity, and pore size distribution. We propose and demonstrate a quicker and much improved method, which offers significant improvement in distinguishing the phases through better image contrast (42%) by *in situ* Pt deposition from the decomposition of a gaseous organometallic

precursor typically available in modern dual-beam scanning electron microscope-focused ion beam (SEM-FIB) instruemnts. As this is a gas-phase deposition, the typical concerns about viscosity associated with epoxy-based methods to ensure percolation are averted as well. We show that the conformal deposition of Pt in the porous carbon electrode allows accurate and fast demarcation of the interfacial boundaries, which in turn enables credible tomographic reconstruction from which the aforementioned geometric structural parameters can be reliably quantified.

MATERIALS AND METHODS

Electrode Fabrication

The porous carbon-based electrodes were prepared following a well-established procedure (Marinaro et al., 2013). Briefly, a suspension of Super-P (Timcal Ltd., Bodio, Switzerland) and Poly(vinylidene fluoride) (Solvay, Bollate (MI), Italy) (Sigma-Aldrich Chemie GmbH, Munich) in N-Methyl-2-pyrrolidone (mass ratio Super-P:PvdF 8:2) was spray-coated using an airbrush on a Gas Diffusion Layer (Toray paper). The layers thus obtained were dried at 100°C in order to allow evaporation of the solvent and polymerization of the binder. Electrodes of 12 mm in diameter were then cut and further dried at 130°C under vacuum, thus minimizing the moisture content. The average loading for all electrodes was of about 1 mg/cm^2 based on the carbon content. For this study, a representative electrode fabricated using this standard fabrication procedure was investigated.

Sample Preparation

The porous carbon-based electrodes were characterized in two different conditions: vacuum impregnated with Si-based resin and *in situ* Pt filled from gaseous precursor.

The porous carbon electrode was vacuum impregnated with Si-based resin ELASTOSIL RT426 catalyzed by T-40 (Wacker Chemie AG, Munich, Germany) and cured at room temperature overnight.

In situ Pt filling of the porous carbon electrode was carried out using the gas injection system mounted on a dual-beam ZEISS N-Vision 40 SEM-FIB system (Carl Zeiss, Oberkochen, Germany). A standard organometallic gaseous precursor ($C_9H_{16}Pt$) was injected in the vicinity of the region-of-interest and by subsequent electron beam-induced dissociation Pt was deposited in the pores. As the depth of deposition is directly proportional to the acceleration voltage of the primary electron beam, it was set to the maximum value of 30 kV for Pt deposition. In this setting, a deposition depth of around 12 μm was obtained. This is more than necessary for tomography, which was limited to a depth of about 3.5 μm. Note that the transition from fully filled to unfilled pores was gradual along the depth direction. Although the electron beam-based deposition is slower than ion-beam deposition, it avoids Ga incorporation in the sample, minimizes the formation of structural defects, and more importantly, has orders of magnitude larger deposition

depth because of the lower electron-sample interaction cross-section. Finally, an additional protective layer of Pt was deposited on the surface on which fiducial markers were engraved by ion milling. These markers helped in subsequent image alignment by cross-correlation to correct for sample drift.

Image Acquisition and Ion Milling

The aforementioned dual-beam ZEISS N-Vision 40 SEM-FIB was employed in this study for imaging and ion milling. The SEM images were acquired at 3 kV. The secondary electron (SE) detector in-lens configuration was used for obtaining the images.

For the tomographic reconstruction of the porous carbon electrode, serial sectioning of the carbon electrode was performed using Ga$^+$ ions with a 30 kV accelerating voltage. The ion-beam axis was at an angle of 54° to the optic axis of the electron beam. The sample stage was tilted in such a way that the ion-beam axis is perpendicular to the sample surface during milling. The slice surface is thus orthogonal to the sample surface. As the SE imaging was performed at an angle of 54°, the voxel size along the y direction was calibrated by using the trigonometric relationship, $y = x/(\sin 54°)$, where the x value was determined by the magnification of the image. More detailed information on FIB tomography is available elsewhere (Uchic et al., 2007).

The x and y dimensions of the voxel of the unprocessed raw image stack were 7.6 and 9.5 nm, respectively. The z dimension of the voxel was determined by the offset between subsequent milling lines for slicing and was more accurately determined by dividing the total milling length in z axis by the number of slices actually milled. In this work, the ion-beam current used for slicing was 80 pA with a slice thickness of 14.7 nm. Subsequently, for the tomographic reconstruction, the image slices were aligned, stacked, and resampled to a voxel size of $10 \times 10 \times 10$ nm^3. The intensity gradient from top to bottom of each slice was corrected by fitting linear functions. Quantification was done using IMOD, ImageJ, and AVIZO software.

RESULTS AND DISCUSSION

Microstructural Characterization

The as-fabricated microstructure of the porous carbon electrode is shown in Figure 1. It can be seen that in addition to the surface, the sub-surface structural features are also in focus due to the larger depth-of-focus of the electron beam. This is a hindrance for tomography reconstructions because the top most surface could not be clearly isolated. Therefore, to unambiguously obtain the surface image, the pores have to be filled to mask the sub-surface features.

Microstructure of the carbon electrode in which the pores were filled with Si-based resin is shown in Figure 2. Although the sub-surface features are masked as expected, we see that the contrast between the carbon electrode (darker features) and the epoxy is rather weak. From line profiles
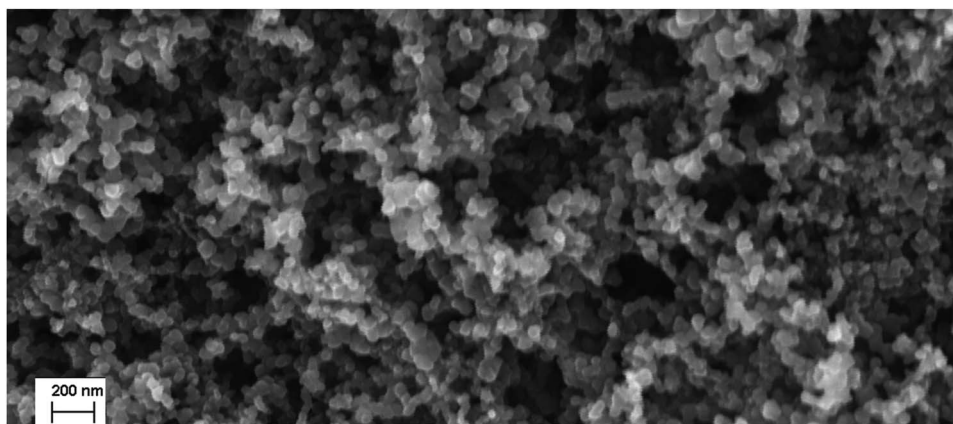
Figure 1. Scanning electron microscopic image of as-fabricated microstructure of porous carbon electrode. Sub-surface features are also visible in the image thereby hindering tomographic reconstruction.
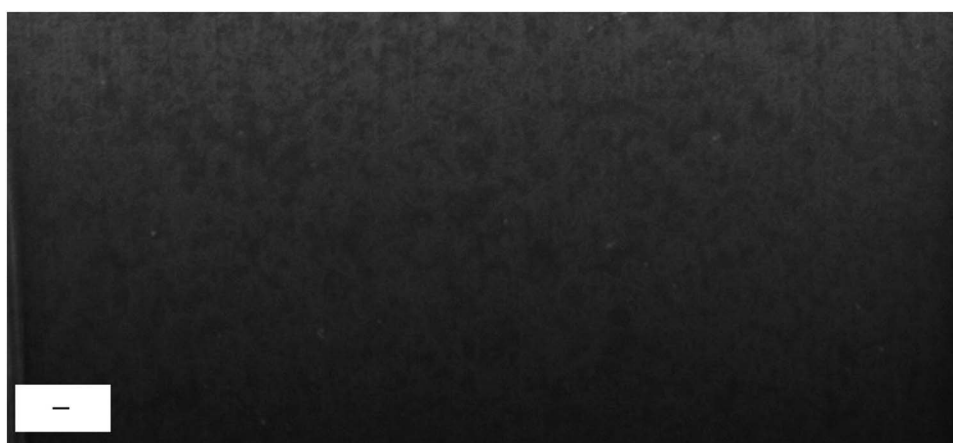

Figure 2. Scanning electron microscopic image of the microstructure of porous carbon electrode vacuum impregnated with Si-based resin. Scale bar is 200 nm.

across the interfaces, the contrast between the two phases, defined as $(I_{max} - I_{min})/I_{max}$ was found to be up to 20%. Although this value is sufficient for qualitative visual understanding of the features, it was found to be insufficient to do robust quantification of microstructural features such as porosity, tortuosity, and pore size distribution because the overlapping grayscales due to weak contrast precludes accurate demarcation of the interfacial boundaries.

The SE image of the *in situ* Pt-filled porous carbon electrode is shown in Figure 3. In comparison with Figure 2, it is readily evident that the contrast in Pt-filled case is drastically higher. From line scan profiles across the interfaces, the contrast was found to be about 42%. With this enhanced contrast, demarcation of the boundaries was easier by application of a grayscale threshold algorithm to distinguish the phases and to assign them to the carbon or pore phase. A few larger partially filled cavities, which were disregarded by the threshold algorithm, were then assigned to the pore phase by using the marker-based watershed algorithm (Meyer & Beucher, 1990). By this semi-automated approach, the phase assignment was successfully and rapidly carried out with very high fidelity.

Microstructural Quantification

Geometric features of the microstructure that were quantified in this study are porosity, tortuosity, pore size distribution, and surface–volume ratio.

Porosity is the ratio of the volume of porous region (Pt filled) to the volume of the entire material under consideration. Numerically, it can be evaluated by dividing the number of voxels corresponding to the pore phase by the total number of voxels. In this way, porosity of the porous carbon electrode was found to be $72 \pm 2\%$.

Tortuosity (τ) is the ratio of the actual length of the pore trajectory between two points (L) and the shortest distance between the same two points (R), i.e., $\tau = L/R$. In addition to this geometric definition of tortuosity, there are also other approaches, for instance, based on effective medium (Ender et al., 2011, 2012). In this study, however, we focus on the geometric definition. Computationally, first the pores in the binarized image stack are represented as an abstract network of lines tracing the medial axes of the pores by a method called topological skeletonization (Sato et al., 2000; Thiedmann et al., 2009) from which length of pore trajectories along
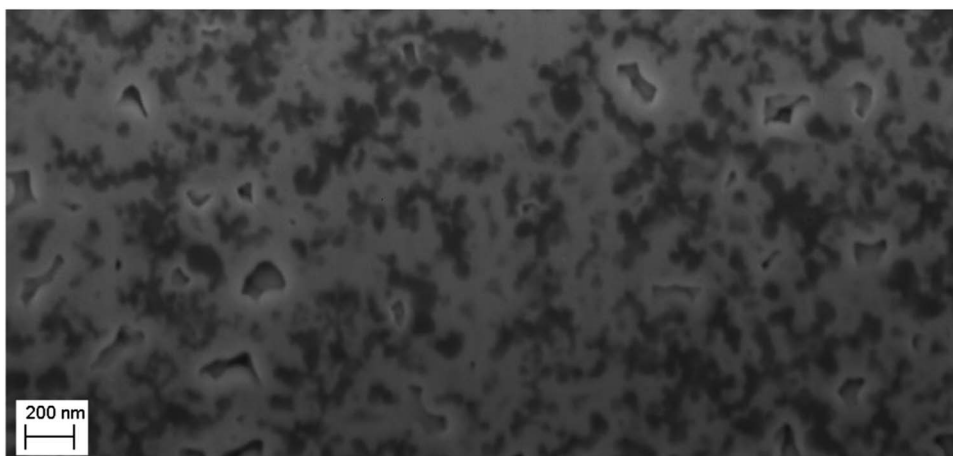
Figure 3. Scanning electron microscopic image of the microstructure of porous carbon electrode (dark features) filled with Pt (light gray) using decomposition of the gaseous organometallic precursor by the electron beam. Note that the larger visible cavities are only partially (yet conformally) filled. They were subsequently digitally filled using the marker-based watershed algorithm and assigned to the pore phase.
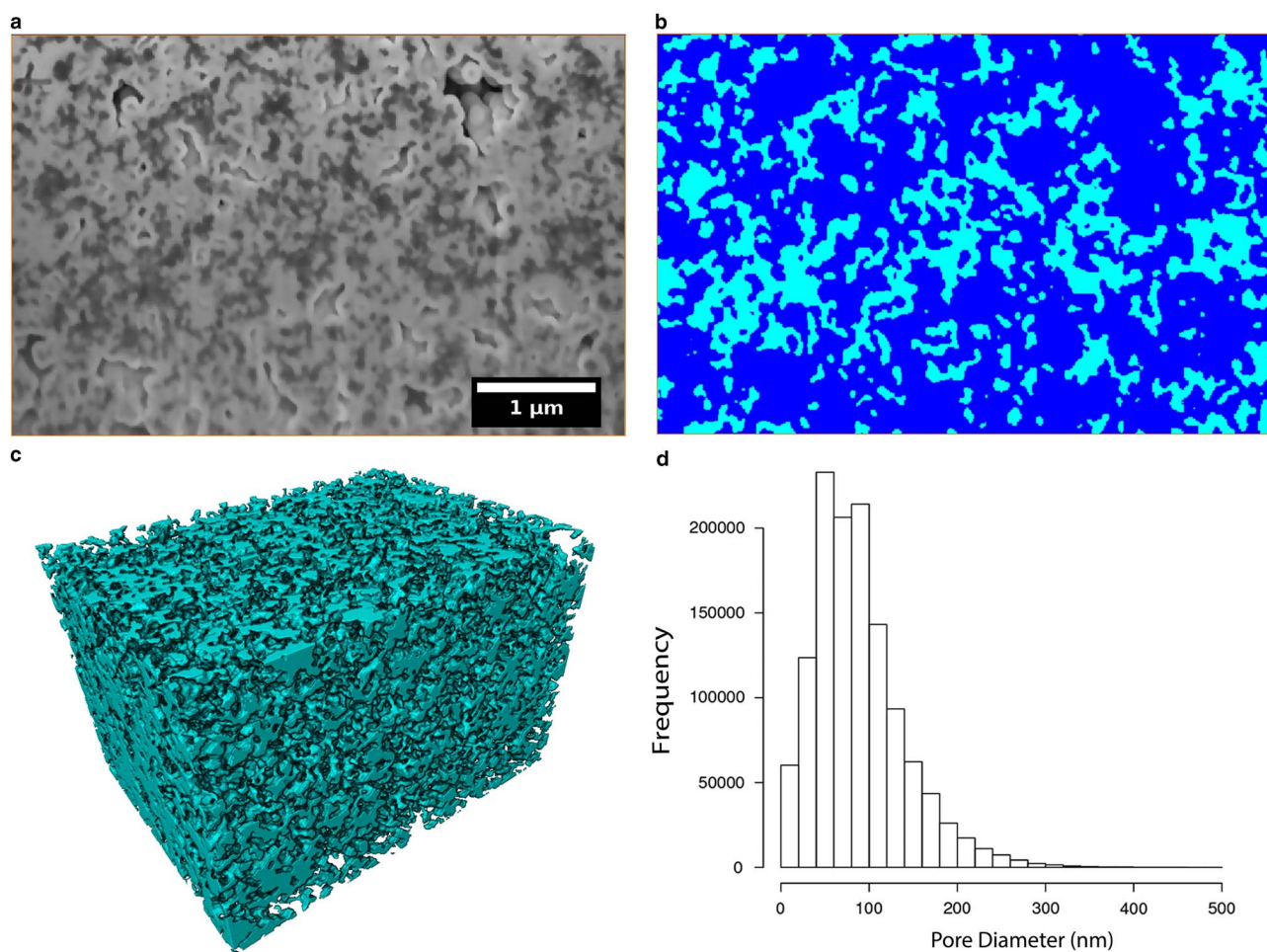

Figure 4. A scanning electron microscopic image slice taken at 3 kV (**a**) and corresponding binarized image (**b**) are shown on top. The carbon phase is shown in turquoise blue in (**b**). Note that very fine features of the porous carbon electrode seen in the raw image have been captured with very high fidelity in the binarized image. **c:** Tomographic 3D reconstruction of the porous carbon electrode. The voxel dimensions are $10 \times 10 \times 10 \, \text{nm}^3$ and the total volume displayed is $5.18 \times 3.38 \times 3.8 \, \mu\text{m}^3$. **d:** The distribution of the pore sizes in the porous carbon electrode.

different directions are obtained. Then, the shortest linear distances between given start and end points of the pore trajectories are calculated using the well-known Dijkstra algorithm (Cormen et al., 2009). With these two quantities, the tortuosities can then be evaluated using the relationship mentioned before.

Using this approach, the tortuosities in the axial direction (normal to the electrode surface) and the radial direction (parallel to the electrode surface) were evaluated and were found to be nearly identical with mean values of 1.45 ± 0.04 and 1.43 ± 0.04, respectively.

Another quantity that can be extracted from the topological skeletonization method is the pore size distribution. The pore radius is obtained by measuring the distance from the medial axis of the pore to the nearest solid boundary at every voxel of the skeletal network (Delerue et al., 1999). The pore size is then given by multiplying the pore radius by a factor of two. In this way, the pore sizes were found to range from 20 nm to more than 300 nm (cavities) with an average pore size of 90 nm. The corresponding plot of the pore size distribution is shown in Figure 4d.

Lastly, we quantified the surface-to-volume ratio, which is an important parameter that has implications for the speed of the electrochemical reactions. The Marching Cubes algorithm (Lorensen & Cline, 1987), which uses a surface-triangulation routine, was employed for determining the surface area and the volume of the carbon phase. The surface-to-volume ratio of the carbon phase was found to be $46.5 \, \mu m^{-1}$ and the specific surface area was determined to be $13.0 \, \mu m^{-1}$. This indicates that the carbon material has a very high surface area, which can be conducive for surface electrochemical reactions.

Conclusion

In this study, we have demonstrated that Pt filling of the pores via gaseous precursors drastically improves the image contrast between the carbon and the porous phases in comparison with the commonly used Si-resin vacuum-impregnation method. The enhanced image contrast enabled robust semi-automatic demarcation of the interfacial boundaries and subsequent binarization of the images with very high fidelity. Tomographic reconstruction of the porous carbon electrode was then obtained by stacking the binarized images. From the 3D reconstruction of the porous carbon electrode, several morphological parameters were then quantified. The porosity was found to be $72 \pm 2\%$. The axial and radial tortuosites were 1.45 ± 0.04 and 1.43 ± 0.04, respectively. The average pore size was evaluated to be 90 nm and the corresponding 1 sigma ranges from 45 to 134 nm. The surface-to-volume ratio and specific surface area were found to be 46.5 and $13.0 \, \mu m^{-1}$, respectively.

Acknowledgment

References

Armand, M. & Tarascone, J.-M. (2008). Building better batteries. *Nature* **451**, 652–657.

Brandon, N.P. & Brett, D.J. (2006). Engineering porous materials for fuel cell applications. *Phil Trans R Soc A* **364**, 147–159.

Cormen, T.H., Leiserson, C.E., Rivest, R.L. & Stein, C. (2009). *Introduction to Algorithms*, 3rd ed. Cambridge, MA: MIT Press.

Delerue, J.F., Perrier, E., Yu, Z.Y. & Velde, B. (1999). New algorithms in 3D image analysis and their application to the measurement of a spatialized pore size distribution in soils. *Phys Chem Earth, Part A* **24**, 639–644.

Ender, M., Joos, J., Carraro, T. & Ivers-Tiffée, E. (2011). Three-dimensional reconstruction of a composite cathode for lithium-ion cells. *Electrochem Comm* **13**, 166–168.

Ender, M., Joos, J., Carraro, T. & Ivers-Tiffée, E. (2012). Quantitative characterization of LiFePO$_4$ cathodes reconstructed by FIB/SEM tomography. *J Electrochem Soc* **159**(7), A972–A980.

García, R.E. & Chiang, Y.-M. (2007). Spatially resolved modeling of microstructurally complex battery architectures. *J Electrochem Soc* **154**(9), A856–A864.

Iwai, H., Shikazono, N., Matsui, T., Teshima, H., Kishimoto, M., Kishida, R., Hayashi, D., Matsuzaki, K., Kanno, D., Saito, M., Muroyama, H., Eguchi, K., Kasagi, N. & Yoshida, H. (2010). Quantification of SOFC anode microstructure based on dual beam FIB-SEM technique. *J Power Sources* **195**(4), 955–961.

Kaiser, J., Simonov, P.A., Zaikovskii, V.I., Hartnig, C., Jörissen, L. & Savinova, E.R. (2007). Influence of carbon support on the performance of platinum based oxygen reduction catalysts in a polymer electrolyte fuel cell. *J Appl Electrochem* **37**, 1429–1437.

Lee, J.-S., Kim, S.T., Cao, R., Choi, N.-S., Liu, M., Lee, K.T. & Cho, J. (2011). Metal–air batteries with high energy density: Li–air versus Zn–air. *Adv Energy Mater* **1**, 34–50.

Long, J.W., Dunn, B., Rolison, D.R. & White, H.S. (2004). Three-dimensional battery architectures. *Chem Rev* **104**, 4463–4492.

Lorensen, W.E. & Cline, H.E. (1987). Marching cubes: A high resolution 3D surface construction algorithm. *ACM Comp Graphics* **21**(4), 163–169.

Marinaro, M., Theil, S., Jörissen, L. & Wohlfahrt-Mehrens, M. (2013). New insights about the stability of lithiumbis (trifluoromethane)sulfonimide-tetraglyme as electrolyte for Li–O$_2$ batteries. *Electrochim Acta* **108**, 795–800.

Meyer, F. & Beucher, S. (1990). Morphological segmentation. *J Vis Commun Image Represent* **1**(1), 21–46.

Sato, M., Bitter, I., Bender, M.A., Kaufman, A.E. & Nakajima, M. (2000). TEASAR: tree-structure extraction algorithm for accurate and robust skeletons. Proceedings of The Eighth Pacific Conference on Computer Graphics and Applications, Hong Kong, pp. 281–449.

Thiedmann, R., Hartnig, C., Manke, I., Schmidt, V. & Lehnert, W. (2009). Local structural characteristics of pore space in GDLs of PEM fuel cells based on geometric 3D graphs. *J Electrochem Soc* **156**(11), B1339–B1347.

Uchic, M.D., Holzer, L., Inkson, B.J., Principe, E.L. & Munroe, P. (2007). Three-dimensional microstructural characterization using focused ion beam tomography. *MRS Bulletin* **32**(5), 408–416.

Uchida, M., Aoyama, Y., Tanabe, M., Yanagihara, N., Eda, N. & Ohta, A. (1995). Influences of both carbon supports and heat-treatment of supported catalyst on electrochemical oxidation of methanol. *J Electrochem Soc* **142**, 2572–2576.